University of Mississippi

eGrove

Breast Cancer Sub-Clones that Metastasize to Lung and Bone Exhibit Different Metabolic Preferences

Mollie Merrell
University of Mississippi

Follow this and additional works at: https://egrove.olemiss.edu/hon_thesis

Part of the Biochemical Phenomena, Metabolism, and Nutrition Commons, Biochemistry Commons, and the Cancer Biology Commons

BREAST CANCER SUB-CLONES THAT METASTASIZE TO LUNG AND BONE
EXHIBIT DIFFERENT METABOLIC PREFERENCES

by

Mollie Merrell

A thesis submitted to the faculty of The University of Mississippi in partial fulfillment of
the requirements of the Sally McDonnell Barksdale Honors College.

Oxford
May 2020

Approved by

_____
Advisor: Dr. Mika Jekabsons

_____
Reader: Dr. Susan Pedigo

_____
Reader: Dr. Wayne L. Gray

ACKNOWLEDGEMENTS

ABSTRACT

Metastasis is responsible for the majority of cancer related deaths. In breast cancer the
lungs and bones are the major sites for metastasis. Previous studies used the metastatic
aggressive MDA-MB-231 breast cancer line to isolate subclones that preferentially
invade the lungs (LM line) or bones (BoM line). While genes associated with the tissue
specific metastasis have been identified, it is unknown if metabolic adaptations contribute
to the growth of the LM and BoM lines in their respective organs. The goal of this study
was to test the hypothesis that the LM and BoM lines exhibit differences in glucose and
glutamine metabolism from their parent MDA-MB-231 breast cancer line. Such
differences would support the broader concept of metabolic plasticity as an important
component of cancer metastasis. We used ^{13}C- metabolic flux analysis with 5-^{13}C
glutamine as the labeled substrate. The rates of glucose uptake, glutamine uptake,
respiration, and lactate production were measured, together with ^{13}C enrichment of
lactate. In parallel, the fraction of glutamine and glucose used for fatty acid synthesis was
assessed with the fatty acid synthase inhibitor C75. The measured fluxes were used to
determine fluxes through glycolysis, the pentose phosphate pathway, the tricarboxylic
acid (TCA) cycle, malic enzyme, and to fatty acids. The LM and BoM cells exhibited
significant metabolic differences from each other and the MDA231 parent line, this
supports our hypothesis and is consistent with such changes contributing to organ-
specific growth of these lines. Specifically, the LM and BoM lines have significantly
lower mitochondrial TCA cycle and respiratory chain activities. The LM cells have a
significantly higher malic enzyme flux, which together with restricted mitochondrial
activity, are proposed to reduce oxidative stress in the high oxygen environment of the

lungs. The BoM cells that metastasize to bones consume significantly less glutamine and have low mitochondrial activity suggesting they rely more heavily on aerobic glycolysis for ATP synthesis in the oxygen-limited bone environment. These metabolic adaptations suggest that organ specific metabolic difference may be a new way to potentially target these cells through development of drugs.

TABLE OF CONTENTS

LIST OF TABLES AND FIGURES

INTRODUCTION

A hallmark of cancer cells is their altered metabolism that was first demonstrated as enhanced glycolytic production of lactate by Otto Warburg. Even when sufficient oxygen is available to fully oxidize glycolytic-derived pyruvate in mitochondria, a greater proportion of pyruvate is instead reduced to lactate; this phenomenon is known as the Warburg effect, or aerobic glycolysis (6). It is thought to have a role in supporting rapid cell proliferation by provision of ATP and/or glycolytic intermediates at a rate sufficient to meet the biosynthetic demands (12). The metabolic demands placed on the anabolic reactions partly depend on the types of concentrations of nutrients that can be imported from the environment (11). For example, cancer cells have high demand for fatty acids to synthesize phospholipids for new membranes. If exogenous fatty acids are limiting, tumors must have the capacity to use glucose and/or glutamine for de novo synthesis. The latter substrate is typically imported at a rate more than ten-fold greater than that of untransformed cells and can be used to re-supply TCA cycle intermediates, and for the synthesis of glutathione, ATP, NADPH and other metabolites important for proliferation (6).

While metastatic cancers often exhibit higher rates of aerobic glycolysis than non-malignant ones, it is unclear if the Warburg effect, or other characteristics of their metabolic phenotype, varies as one or a few cells preferentially invade and grow in different secondary tissues (10). Each secondary site represents a potentially distinct microenvironment that may necessitate subtle adjustments in the tumor's metabolic phenotype for success (7). Besides distinct tissue microenvironments, metastasis to one or more secondary sites depends on genetic heterogeneity within the primary tumor.

Transcriptomics studies have been performed on the MDA-MB-231 breast cancer line that commonly metastasizes to the bones and lungs (7). Highly selective bone or lung metastasizing subclones (denoted BoM and LM lines, respectively) were developed from injections of MDA-MB-231 cells into mice; lung and bone tumors were iteratively isolated, expanded in culture then re-introduced in mice until the resulting lines exclusively invaded either the lungs or bone when injected into immune deficient mice (7, 8). The bone metastatic cells were not able to grow in the lungs demonstrating that metastatic cells that grow well in one location may not grow well at another (8). In the bone cell lines overexpression of interleukin-11(IL-11) and osteoponitin (OPN) with the addition of chemokine receptor 4 (CXCR4) increases bone metastasis activity (10). In the MDA-MB-231 cell line 10% of the cells contained CXCR4 which was in the bone metastasis gene expression. When looking at the gene set for lung expression there was only six genes the overlapped with the bone metastasis gene expression (7). Overexpression of SPARC and ID1 significantly associated with metastasis to lung (10). When examining the primary breast cancer tumors those expressing the lung metastasis signature had higher activity while the bone metastasis signature did not (7). There are no genes found that are overexpressed in LM or BoM that participate in metabolic pathways. However, this does not eliminate the possibility of metabolic differences between these cell lines.

We hypothesized that tissue-specific metastasis is associated with subtle differences in metabolic reprogramming of glucose and glutamine metabolism to allow continued proliferation and invasion in different organ microenvironments. Metabolic differences in the cell lines could be because the microenvironment of the new organ to

which they invade is different from where the tumor originally grew. Therefore, the aim of the study was to determine whether the LM and BoM subclones have metabolic variations relative to the original breast cancer line from which they are derived. In order to test this hypothesis, we used a combination of pharmacological inhibitor studies and ^{13}C lactate labeling experiments with 5-^{13}C glutamine.

METHODS

A. Cell lines and culture

Metastatic breast cancer MDA-MB-231 cells (hereafter referred to as MDA231) and the less aggressive T47D breast cancer cells were provided by Dr. Y.D. Zhou (University of Mississippi, Department of Chemistry and Biochemistry). Sub-clones of MDA231 cells that preferentially metastasize in lung (LM) and bone (BoM) were generated by Massague's lab (7,14). Both LM and BoM cells were obtained from Dr. Kounosuke Watabe (Wake Forest University) and provided by Dr. Zhou. Cells were routinely cultured using RPMI-1640 media supplemented with 10% fetal bovine serum and 0.5% vol/vol penicillin-streptomycin in 10 cm polystyrene petri dishes at 37°C in a humidified 5% CO_2 incubator. Cells were maintained in culture for no more than 20 passages, and typically split twice a week. The day before each experiment, approximately 1.0 x 10^6 cells were seeded in each well of 2-well Lab-Tek chambers. Control wells received 2mL standard cell culture media while treatment wells were incubated in glutamine-free RPMI-1640 media supplemented with 1.5 mM 5-^{13}C glutamine. Cells were incubated for 20-22 hours prior to experiments.

B. Materials (reagents)

Glutamate pyruvate transaminase, glucose-6-phosphate dehydrogenase (G6PDH), lactate dehydrogenase, nicotinamide adenine dinucleotide phosphate (NADP), nicotinamide adenine dinucleotide (NAD), adenosine triphosphate (ATP), and 2 oxoglutarate were purchased from Calzyme (San Luis Obispo, CA). Hexokinase, microbial glutamate dehydrogenase, 3-nitrophenylhydrazine, and N-(3-dimethylaminopropyl)-N'-ethylcarbodiimide (EDC) were purchased from Sigma (St.

Louis, MO). Glutaminase was purchased from Megazyme (Chicago, IL). 5-^{13}C glutamine was purchased from Cambridge Isotopes (Tewksbury, MA). Cell culture media, fetal bovine serum, and cell culture supplies were purchased from Fisher Scientific (Pittsburg, PA). Buffers and other general reagents were purchased from Sigma.

C. Flux experiments

After overnight incubation in cell culture media ± 5-^{13}C glutamine, cells were rinsed then equilibrated 5 h 37°C in experimental buffer containing 137 mM NaCl, 5 mM KCl, 20 mM TES, 1.3 mM CaCl$_2$, 1.3 mM MgCl$_2$, 1.2 mM Na$_2$SO$_4$, 0.4 mM KH$_2$PO$_4$, 0.2 mM NaHCO$_3$, 5.5 mM glucose, 0.3 % fatty acid-free bovine serum albumin (BSA), ± 1.5 mM 5-^{13}C glutamine, pH 7.4. For some experiments, 40 μM C75 (an inhibitor of fatty acid synthase) was included in buffer containing 1.5 mM unlabeled glutamine to estimate the proportion of glucose and glutamine used for fatty acid synthesis. The control buffer contained no glutamine. Respiration rate of cells in each well was determined at 37°C in 2.15 mL fresh buffer using a custom-made setup with a Clark-type micro-oxygen electrode (Micrelectrodes, Inc., Bedford MA) (Fig. 2). Data for each well was acquired over 45-55 min. with a Powerlab A/D unit and Lab Chart software (AD Instruments). Cells were rinsed once with buffer then serially incubated for 60 min, 120 min, and 60 min at 37°C with 350 μL buffer. After each incubation period, buffer was collected in microfuge tubes on ice, the cells were rinsed once, and then 350 μL buffer added for the next incubation period. Control wells without cells were incubated in parallel to correct for evaporative volume changes over each incubation period. The samples were centrifuged for 5 min. 4°C at 21,000 xg and supernatants stored at -20°C for metabolite assays and mass spectrometry. The 60 min. incubations were used to assess average rates

5

of glucose consumption and lactate production, while all three were used to assess glutamine consumption. Cell pellets were visible for the MDA231 samples; these were saved and assayed for protein content to correct for protein loss over each incubation period. After the final incubation, wells were rinsed once with 1 ml phosphate buffered saline (PBS) then solubilized for 15min at 37°C with 500 μL 50 mM NaCl, 20 mM TES, 1% SDS, pH 7.3. The extracts were vortexed 2-3 min. then centrifuged 10 min. 21,000xg 10°C and the supernatants stored at -20°C for protein assay. The MDA231 cell pellets were washed once with 200 μL PBS, repelleted by centrifugation, then solubilized with 100 μL SDS buffer and stored at -20°C.
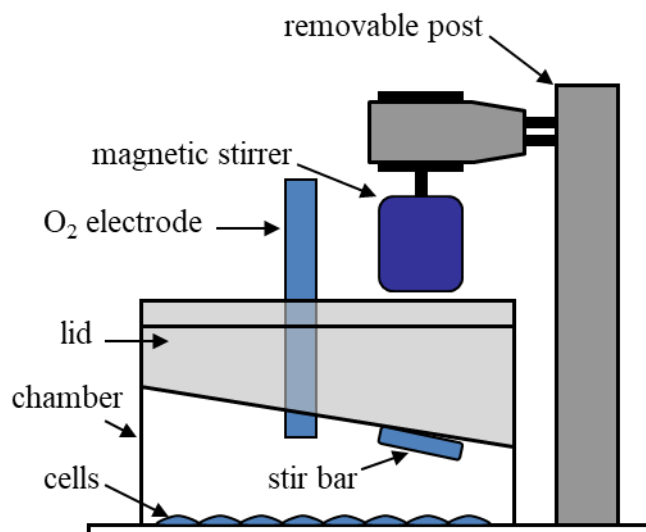

Figure 1: This figure shows the set up for respiration measurement. Shown are the cells plated at the bottom of chamber. A stir bar located in the media is being turned by a magnetic stirrer on the other side of the cell chamber lid. In the container is an O₂ electrode which measures the decreasing oxygen concentration of the buffer.

D. Metabolite assays

D.1. Glucose Assay

The samples and standards (5 μl; run in triplicate) were added to 115 μl buffer

containing 100 mM triethanolamine, 7 mM $MgCl_2$, 2 mM ATP, 2 mM NADP, 1 U/ml

hexokinase, and 1 U/ml glucose-6-phosphate dehydrogenase, pH 7.3. Reduction of

NADP to NADPH occurs as glucose is oxidized over the 8-10 min incubation period.

The resulting samples were measured in a Shimadzu RF6000 spectrofluorophotometer

(λex = 341 nm, λem = 464 nm).

D.2. Glutamine Assay

The samples and standards (6 μl; run in duplicate) were added to 34 μl buffer

containing 60 mM sodium acetate pH 4.9 with or without 1 U/ml glutaminase.

Glutaminase was used to convert glutamine to glutamate by cleaving the amino group to

release free ammonia. The samples were incubated in a water bath (37°C) for 45 minutes.

After the incubation, the samples were added to another buffer which contained 300 mM

TRIS, 10 mM 2-oxoglutarate, 240 μM NADPH, and 2 u/mL of glutamate dehydrogenase.

The glutamate dehydrogenase catalyzed the reductive amination of 2-oxoglutarate to

glutamate using the free ammonia generated by the glutaminase reaction. This was

incubated for 1 hour and 30 minutes at room temperature in the dark because NADPH is

light sensitive. The samples were then measured in a Shimadzu RF6000

spectrofluorophotometer (λ_{ex} = 341 nm and λ_{em} = 464 nm). Our cells naturally produce

ammonia so to differentiate we run the standard without glutaminase and subtract the

NADPH fluorescence's.

D.3. Lactate Assay

The samples and standards (5 μl; run in triplicate) were added to 115 μl buffer

containing 100 mM glycylglycine, 100 mM glutamate, 2 mM NAD, 1 U/ml lactate

dehydrogenase, and 1 U/ml glutamate-pyruvate transaminase, pH 8.5. In this reaction (40 min), lactate is oxidized to pyruvate, NADH is produced, and pyruvate is removed by transamination to facilitate conversion o f lactate to pyruvate. The samples were measured in a Shimadzu RF6000 spectrofluorophotometer (λex = 341 nm, λem = 464 nm).

D.4. Protein Assay

Quantitation of total protein in soluble cell extracts (duplicates, diluted 1:3 in water) were determined by bicinchoninic acid (BCA) assay. Reactions (25 µl sample with 500 µl BCA reagent) were incubated for 30 min, 60°C, cooled, and quantitated at 562nm using a Ultrospec 3100pro spectrophotometer (Amersham Biosciences). Bovine serum albumin standards (0, 50, 100, 150, 200, 300, 400, and 500 ug/ml) dissolved in solubilization buffer were run in parallel. Additionally, protein assays were run for the MDA cell pellets to correct for protein lost over each incubation period. The MDA cells have a much lower adherence to the plate than the three other lines. Due to this inequality MDA cells were spun into pellets and assayed to measure the protein content as a form of compensation to account for the cell loss during the experiment.

E. Lactate derivatization and mass spectrometry analysis of 13C lactate

UHPLC–MS/MS of derivatized lactate

The samples and lactate standards (14 µl) were extracted with 2 volumes 100% cold methanol and then incubated for 1 H , -20°C, to precipitate buffer proteins. The samples were then centrifuged at 21,000 xg, 2°C for 10 min. The resulting supernatant was then transferred to new tubes. Next the reagents 50 mM EDC (prepared fresh in 1.5% pyridine, 98.5% ethanol, 21 µl) and 140 mM NPH (prepared fresh in 50% ethanol, 21 µl)

were added to the tubes in that specific order to derivatize lactate with 3-nitrophenylhydrazine. The reaction was incubated for 2 h, 37°C, and then cooled on ice. The samples (30 µl) were then diluted in 970 µl 80% methanol in mass spec vials for analysis by liquid chromatography-triple quadrupole mass spectrometry. Both unlabeled (M), 13C labeled (M1), and 66:1 M:M1 lactate standards were run to confirm the expected masses (224 Da for M, 225 Da for M1) and verify separation of these isotopologues.

The derivatized samples were separated on a Waters ACQUITY I-Class UPLC™ system including binary solvent manager, sample manager and column manager connected to a Waters Xevo TQ-S triple quadrupole mass spectrometer (Waters Corp, Milford, MA, USA). The separation was carried out on a Waters Acquity UPLC™ BEH C18 column (50mm × 2.1mm i.d., 1.7 µm). The sample temperature and column temperature were maintained at 10 °C and 40 °C, respectively. The mobile phase consisted of water containing 0.1% formic acid (v/v) (A) and acetonitrile with 0.1% formic acid (B). The analysis was performed using the following gradient elution at a flow rate of 0.50 mL/min: 0-2.5 min, 5% B to 18% B; 2.5-3 min, 18% B to 100% B. Each run was followed by a 2.5 min wash with 100% B and an equilibration period of 2.5 min with the initial conditions. The strong and weak solutions used to wash the auto sampler were methanol/acetonitrile/isopropanol/water (25:25:25:25, v/v/v/v/v) and methanol/water (70:30, v/v), respectively. The injection volume was 1 µl. The UHPLC effluent was introduced into the Waters Xevo TQ-S mass spectrometer equipped with electrospray ionization in negative ion mode (ESI-) for quantification of the analytes. Detection was obtained by Multiple Reaction Monitoring (MRM) mode including two MRMs for confirmation of the analytes. MRM transitions and related parameters are listed in Table 1.

The quantification of analytes 224, 225, 226, and 227 (the expected masses for M, M1, M2, and M3 lactate derivatized with nitrophenylhydrazine, respectively) was acquired with transitions of deprotonated ion at m/z 224.04 → 152.06 for M, 225.04 → 152.06 for M1, 226.04 → 152.06 for M2, and 227.04 → 152.06 for M3 with dwell time of 20 msec at cone voltage 44 V and collision energy 14 eV for each transition. The ESI–MS/MS parameters were set as follows: capillary voltage, 1.20 kV; cone voltage, 44 V; source temperature, 150 °C; desolvation temperature, 600 °C; desolvation gas flow, 600 L/h, cone gas flow, 200 L/h. Nitrogen was used as desolvation and cone gas. Argon (99.99% purity) was introduced as the collision gas into the collision cell at a flow rate of 0.15 mL/min. Data acquisition was carried out by MassLynx 4.1 software and processed by TargetLynx (Waters Corp., Milford, MA, USA).

Table 1 Optimized UHPL-MS/MS parameters for each analyte

Analyte	[M-H]$^-$ (*m/z*)	MRM transition (*m/z*)	Cone votage (V)	Collision energy (eV)	Retention time (min)
M	224.04	224.04 -> 152.06 224.04 -> 137.11	44	14 22	1.84
M1	225.04	225.04 -> 152.06 225.04 -> 137.11	44	14 22	1.84
M2	226.04	226.04 -> 152.06 226.04 -> 137.11	44	14 22	1.84
M3	227.04	227.04 -> 152.06 227.04 -> 137.11	44	14 22	1.84

F. Flux Calculations

For ^{13}C glutamine experiments, measured fluxes include glucose uptake (J_0), lactate production (J_4), mitochondrial respiration rate (J_{RR}), and external glutamine consumption (J_{10}). For C75 experiments, the fraction of glucose or glutamine used for fatty acid synthesis $1 - \frac{J\,C75}{J\,cntl}$, and the fraction of C75-senstive glucose diverted to lactate

for ATP synthesis $\frac{0.5(J_4cntl - J_4C75)}{J_0cntl - J_0C75}$ were measured. These data, along with ^{13}C enrichment

in lactate, were the basis for assessing all intracellular fluxes using a Microsoft Excel-

based computational model to optimize the following parameters: malic enzyme (J_7)

contribution to total pyruvate produced, $\frac{J_7}{J_{2c}+J_7} = X$ (where J_{2c} = glycolytic flux from 3-

phosphoglycerate to pyruvate) , glutamate dehydrogenase (J_{11}) contribution to total

alpha-ketoglutarate produced, $\frac{J_{11}}{J_{11}+J_{12f}} = Y$, and the fraction of exogenous glutamine

oxidized to α-ketoglutarate, $\frac{J_{11}}{J_{10}} = Z$. The 14 fluxes not measured can be calculated from

the measured fluxes and model-optimized parameters as detailed below, provided that the

cells maintain a metabolic steady-state (i.e., the production and consumption of each

metabolite is equal). Mitochondrial respiration rate was not directly used to calculate

fluxes, but was important in providing constraints for calculation of fluxes through the

TCA cycle reactions.

Given that the model finds the solution $\frac{J_{11}}{J_{10}} = Z$ it follows that the rate of

glutamate oxidation to αKG is calculated as:

$$J_{11} = J_{10} \cdot Z \tag{Eq.1}$$

The reductive carboxylation of αKG to citrate (J_{12r}) for fatty acid synthesis is calculated

from the C75-sensitive glutamine consumption:

$$J_{12r} = J_{10} * (1 - \frac{J_{10}C75}{J_{10}cntl}) \tag{Eq. 2}$$

Given the solution $\frac{J_{11}}{J_{11}+J_{12f}} = Y$, the forward oxidation of citrate to αKG is calculated by

solving for J_{12f}:

$$J_{12f} = \frac{J_{11}(1-Y)}{Y} \tag{Eq.3}$$

11

The glucose consumption for fatty acid synthesis was calculated by subtracting the C75-sensitive glucose converted to lactate from the total C75-sensitive glucose uptake:

$$glc \ for \ FA = 0.36 * [J_0 * \left(1 - \frac{J_0 C75}{J_0 cntl}\right) - 0.5 * J_0 * \left(\frac{J_4 cntl - J_4 C75}{J_0 cntl - J_0 C75}\right)] \quad \text{(Eq. 4)}$$

Equation 4 assumes that 11 glucose are required to synthesize each palmitate; four (36%) are used as the carbons for the fatty acid and seven (64%) are used by the oxidative PPP to generate the 14 NADPH required for palmitate synthesis. The rate of citrate used for fatty acid synthesis is thus:

$$J_{13} = J_{12r} + 2 * (glc \ for \ FA) \quad \text{(Eq. 5)}$$

From the citrate balance, the total rate of pyruvate oxidation to citrate (J_5) is:

$$J_5 = J_{12f} + J_{13} - J_{12r} \quad \text{(Eq. 6)}$$

The malic enzyme flux (J_7) is determined from the model-optimized ratio $\frac{J_7}{J_{2c}+J_7} = X$ and the relationship $J_{2c} + J_7 = J_4 + J_5$. Substituting:

$$J_7 = X * (J_4 + J_5) \quad \text{(Eq. 7)}$$

From the pyruvate balance, lower glycolytic flux (J_{2c}) is:

$$J_{2c} = J_4 + J_5 - J_7 \quad \text{(Eq. 8)}$$

3-phosphoglycerate flux to serine was assumed to be negligible, so flux from the triose phosphates to 3-phosphoglycerate (J_{2b}, middle glycolysis) is:

$$J_{2b} = J_{2c} \quad \text{(Eq. 9)}$$

Since the stoichiometry of NADH produced per 3-phosphoglycerate produced is 1:1, the rate of glycolytic NADH production $= J_{2b}$. Mitochondrial oxidation of glycolytic NADH (J_6, via the malate-aspartate shuttle) is thus the residual NADH not used to reduce pyruvate to lactate:

$$J_6 = J_{2b} - J_4 \quad \text{(Eq. 10)}$$

The glucose used for both the oxidative and non-oxidative pentose phosphate pathway for NADPH and ribose-5-phosphate synthesis is the difference between the measured glucose uptake and the rate of glycolytic production of 3-phosphoglycerate (J2b, in glucose units):

$$J_{PPP} = J_0 - 0.5 * J_{2b} \qquad \text{(Eq.11)}$$

The rate of αKG oxidation to succinate can be calculated from the αKG mass balance:

$$J_{14} = J_{11} + J_{12f} - J_{12r} \qquad \text{(Eq.12)}$$

Succinyl CoA consumption outside the TCA cycle was assumed to be negligible, so:

$$J_{15} = J_{14} \qquad \text{(Eq.13)}$$

The rate of malate to OAA can be determined from the malate mass balance:

$$J_{16} = J_{15} - J_7 \qquad \text{(Eq.14)}$$

The citrate-derived oxaloacetate regenerated by fatty acid synthesis from glucose-derived pyruvate was assumed to return to the TCA cycle, so that:

$$J_{17} = J_{16} + 2 * (glc\ for\ FA) \qquad \text{(Eq.15)}$$

RESULTS

A. Theory on predicting ^{13}C lactate enrichment from 5-^{13}C glutamine to assess TCA cycle and malic enzyme activity

Glutamine supports the growth of many tumors as an anapleurotic and/or bioenergetic substrate for the TCA cycle. The proportion of glutamine entering the TCA cycle can be followed by ^{13}C tracer analysis in one or more downstream metabolites. For this study, we labeled cells with 5-^{13}C glutamine and assessed downstream enrichment in lactate exported to the experimental buffer. Enrichment in lactate was chosen as a means to quantify fluxes through TCA cycle and malic enzyme reactions. Upon being taken up by the cell, glutamine is deaminated to glutamate and then enters the TCA cycle by oxidation to α-ketoglutarate (αKG), where the labeled carbon is retained at position 5 in this metabolite (Fig. 2). Decarboxylation of carbon 1 occurs by αKG dehydrogenase, resulting in succinyl-CoA that retains the labeled carbon at position 4. Coenzyme A is removed by succinate thiokinase, which yields the symmetrical product succinate; since succinate dehydrogenase cannot distinguish between carbons 1 and 4, 50% of succinate is ^{13}C labeled at position 1 and 50% at position 4. The product fumarate is also symmetrical, so the labeling pattern is retained as fumarate is converted to the non-symmetrical product malate. From here there are two different routes that can be taken: First, malic enzyme can decarboxylate carbon 4 of malate to generate pyruvate so only 50% of pyruvate generated in this way is expected to be labeled at carbon 1. Metabolism of unlabeled glucose through glycolysis yields unlabeled that is assumed to mix with the malic enzyme-derived pyruvate. Some of this pyruvate can be reduced to lactate to give the same labeling pattern- single (M1) labeled lactate. Alternatively, some malate carbons

14

are oxidized to oxaloacetate (OAA) such that the labeled carbons are retained in the same order. Citrate synthase then catalyzes a condensation reaction with acetyl CoA from pyruvate to form citrate, but since carbon 1 of pyruvate is lost upon conversion to acetylCoA, citrate is labeled at either carbons 5, or 6,. Reductive carboxylation of 5-^{13}C αKG to citrate can also yield citrate labeled at carbon 1. As citrate is oxidized to αKG the label at carbon 6 is removed. Therefore, as the second turn of the cycle begins, αKG labels occur at position 5 and position 1. However, when αKG labeled at carbon 1 is oxidized to succinyl-CoA carbon 1 is lost. Therefore, the labeling pattern of succinyl-CoA after the first turn of the cycle is not expected to change, so double (M2) and triple (M3) ^{13}C lactate labeling is not expected to occur.

The extent of M1 lactate enrichment partly depends on the contribution of glutamate dehydrogenase (J_{11}) to generating αKG:

$$\frac{J_{11}}{J_{11}+J_{12f}} \qquad \text{(Ratio 1)}$$

Lactate M1 enrichment also depends partly on the contribution of malic enzyme (J_7) to pyruvate production:

$$\frac{J_7}{J_{2b}+J_7} \qquad \text{(Ratio 2)}$$

Therefore, a computational model was developed in which Eqs. 16 and 17 were developed as optimized parameters that were varied by the Solver function in Excel to reproduce the measured ^{13}C lactate enrichment as close as possible.

The fraction of glutamine entering the TCA cycle

$$J_{11}/J_{10} \qquad \text{(Ratio 3)}$$

15

was also incorporated in the model because mitochondrial respiration rate imposes a

constraint on the reducing equivalents NADH and FADH$_2$ generated by the TCA cycle as
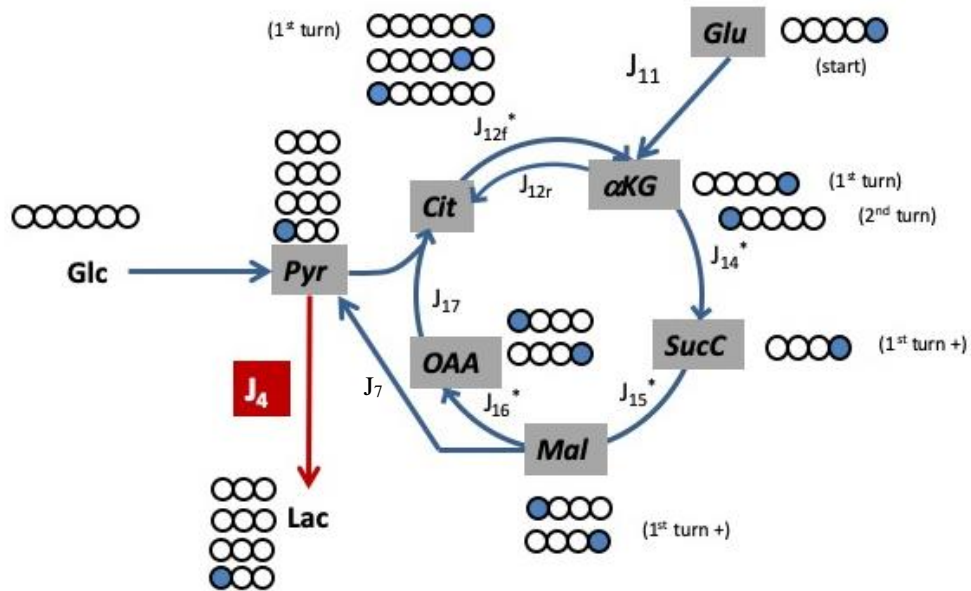
glutamine is oxidized.

Figure 2: ^{13}C distribution in first and second turn of the TCA cycle with [5-^{13}C] glutamine. The labeling scheme begins with [5-^{13}C] glutamine as it enters the TCA cycle upon glutamate (Glu) oxidation (J_{11}). The colored circles indicate ^{13}C labeled atoms and the open circles indicate ^{12}C atoms. The carbons are numbered starting with position 1 on the left. ^{13}C glutamine enters the cycle labeled at position 5 as glutamate is oxidized to α-ketoglutarate (αKG). As the glutamine carbons travel around the TCA cycle to malate (Mal), which is then oxidized by malic enzyme (J_7) to pyruvate (Pyr), 13C enrichment in lactate (Lac) is expected only at carbon 1. Recycling of ^{13}C as oxaloacetate (OAA) forms citrate (Cit) (J_{17}) is not expected to yield additional labeling of succinylCoA (SucC) or malate during subsequent turns of the cycle.

B. Glucose and glutamine for fatty acid synthesis

Rapidly dividing tumor cells have high demand for fatty acids to synthesize

phospholipids for new membranes. Exogenous fatty acids may be limiting, so many

tumors must use glucose and/or glutamine for de novo synthesis. To assess the proportion

of glucose and glutamine used to synthesize fatty acids and the overall rate of fatty acid

synthesis, tumor cells were treated with the fatty acid synthase (FAS) inhibitor C75.

When FAS is inhibited there should be less demand for glucose and/or glutamine;

therefore, the rate of glucose and/or glutamine uptake from the media should decrease, and the extent of the change (the C75-sensitive consumption) should provide an index of the rate at which these substrates are used for fatty acid synthesis. Results from these experiments were combined with those using $5\text{-}^{13}C$ glutamine as detailed in Section F of the Methods section.

Cells were preincubated in experimental buffer $\pm$ 40 µM C75 for 4 h and then glucose and glutamine consumption were assessed over three sequential incubation periods (1, 2, and 1 h). By 2-way ANOVA (cell line and C75 treatment as main effects), there was a borderline significant main effect of C75 treatment on glucose (p=0.0496) uptake (Fig. 3), suggesting that glucose may be used to synthesize fatty acids in these cell lines. Glucose consumption was most affected in the T47D and MDA231 lines; the rates with C75 were 81.6±4.7% (n=4; p=0.02 by one-tailed t-test) and 80.6±2.8% (n=3; p=0.02 by one-tailed t-test), respectively, of the controls (Fig. 3). In contrast, BoM and LM rates were not significantly reduced (glucose consumption with C75 was 97.1±4.8%, n=4, p=0.31 and 92.1±5.6%, n=3, p=0.15, of the respective BoM and LM controls). Lactate production rate was also measured to determine if the decrease in glucose uptake rate can be explained by a reduction in aerobic glycolysis; this could occur if inhibiting fatty acid synthesis secondarily reduces ATP consumption, which in turn could affect glycolytic rate. Consistent with this possibility, lactate production tended to be lower in the T47D, MDA, and LM lines (Fig. 4), although there was no significant main effect of C75 (p=0.61 by 2-way ANOVA). Reduced aerobic glycolysis accounted for 33.7±13.8%, 23.9±12.8%, and 78.0±22.4% of C75-sensitive glucose uptake for LM, MDA, and T47D lines, respectively. After accounting for the reduction in glucose converted to lactate for

these 3 lines, and for the stoichiometry of palmitate synthesis from glucose (see Eq. 4), the absolute and normalized rates of glucose diverted to fatty acids did not significantly differ ($p=0.09$, $p=0.20$, respectively by 1-way ANOVA) between the cell lines (Fig. 6). MDA cells notably had a higher glucose consumption rate (Fig. 6A) and a higher proportion of glucose diverted to fatty acids (Fig. 6B), but the variability in these measurements were too great to yield significant differences.

Inhibition of FAS had more pronounced effects on glutamine consumption ($p<0.0001$ for main effect of C75 by 2-way ANOVA), suggesting that glutamine is the preferred substrate for fatty acid synthesis. Glutamine consumption was significantly reduced to similar extents in T47D ($68.1\pm4.4\%$ of controls, n=4, $p=0.002$), MDA ($68.4\pm8.2\%$ of controls, n=3, $p=0.026$) and BoM ($69.7\pm6.0\%$ of controls, n=4, $p=0.014$) lines, while LM cells were modestly affected ($90.8\pm4.4\%$ of controls, n=3, $p=0.087$). The C75-sensitive glutamine consumption rates did not significantly differ between the lines ($p=0.12$ by 1-way ANOVA; Fig. 7A); however, the lines significantly differed in the proportion of glutamine diverted to fatty acids ($p=0.01$ by 1-way ANOVA). LM cells diverted a significantly less ($9.2\pm4.4\%$) glutamine to fatty acids compared to T47D ($31.9\pm4.4\%$), MDA ($31.6\pm8.2\%$), and BoM ($30.3\pm6.0\%$) cells (Fig. 7B).
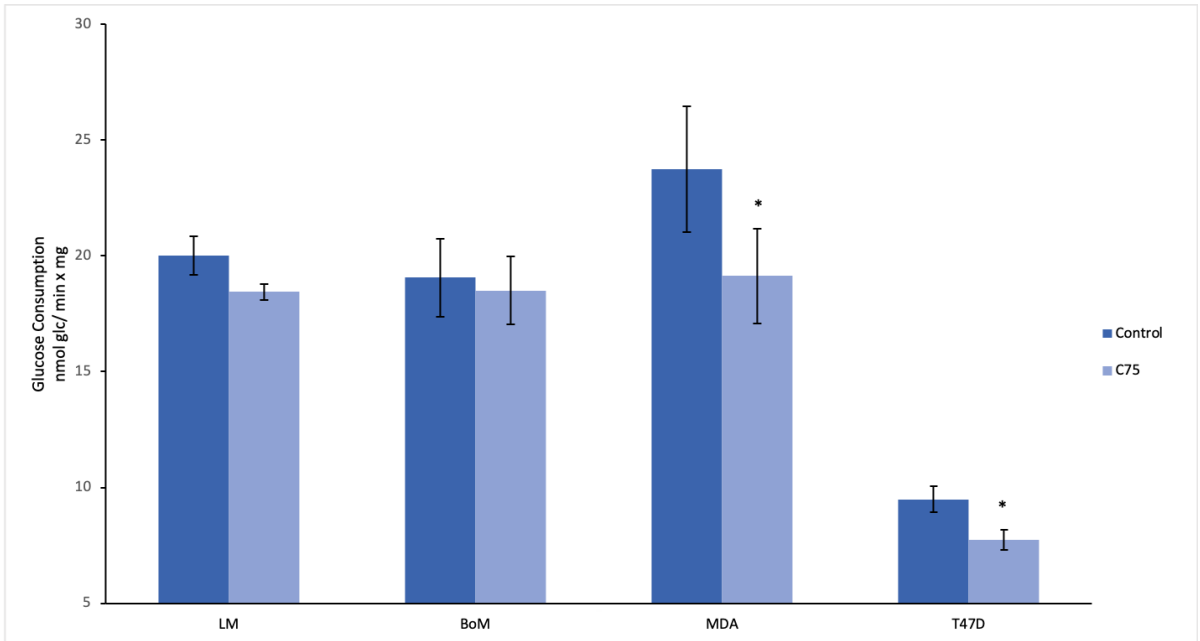
*Figure 3 Effect of C75 on glucose uptake: Cells were incubated for 4 hours at 37℃ with or without 40 µM C75 and glucose uptake was determined over three sequential 1-2 hr incubations. Glucose concentrations were measured by enzymatic assays as described in the methods. Data are mean ± standard error of three (LM, MDA231) or four (BoM, T47D) independent experiments. Asterisks * denote p< 0.05 compared to corresponding control by t-test.*
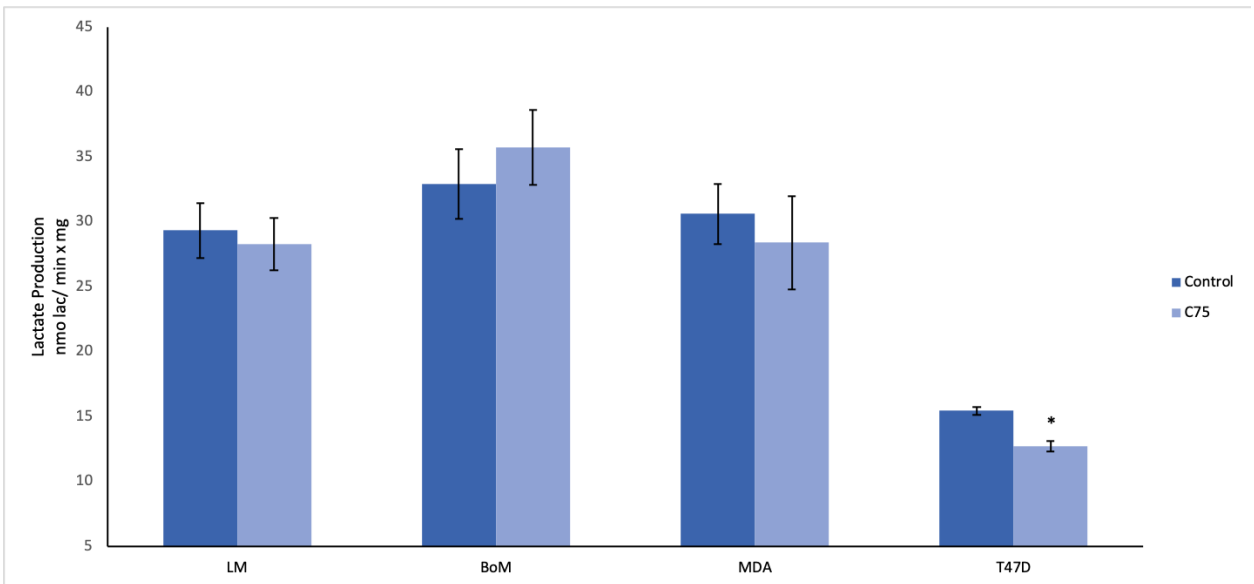
*Figure 4 Effect of C75 on lactate production: Cells were incubated for 4 hours at 37℃ with or without 40 µM C75. Lactate concentrations were measured by enzymatic assays as described in the methods. Data are mean ± standard error of three (LM, MDA231) or four (BoM, T47D) independent experiments. Asterisks * denote p< 0.05 compared to corresponding control by t-test.*

*Figure 5 Effects of C75 on glutamine consumption: Cells were incubated for 4 hours at 37°C with or without 40 μM C75. Glutamine concentrations were measured by enzymatic assays as described in the methods. Data are mean ± standard error of three (LM, MDA231) or four (BoM, T47D) independent experiments. Asterisks * denote p< 0.05 compared to corresponding control by t-test.*
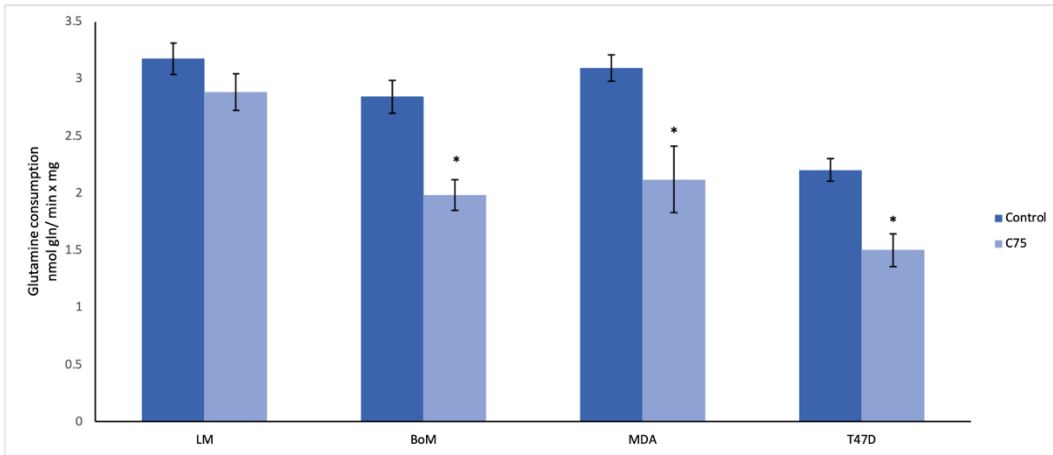

Figure 6 Absolute and fractional rates of C75-sensitive glucose diverted to fatty acids: (A) The absolute rates of C75-senstive glucose to fatty acid were determined after subtracting the rate of C75-sensitive glucose converted to lactate. One-way ANOVA indicated no significant cell line effect (p=0.09) (B) The absolute rates in (A) were normalized to the rates of glucose uptake for the controls. One-way ANOVA indicated no significant cell line effect (p=0.20).
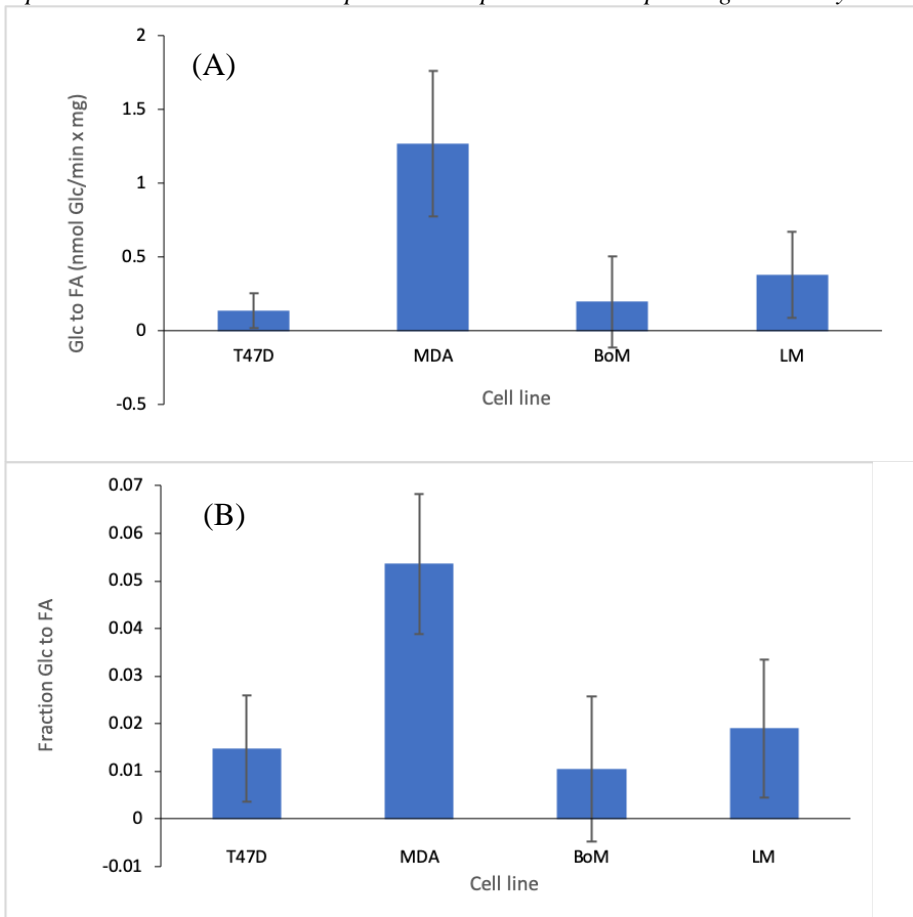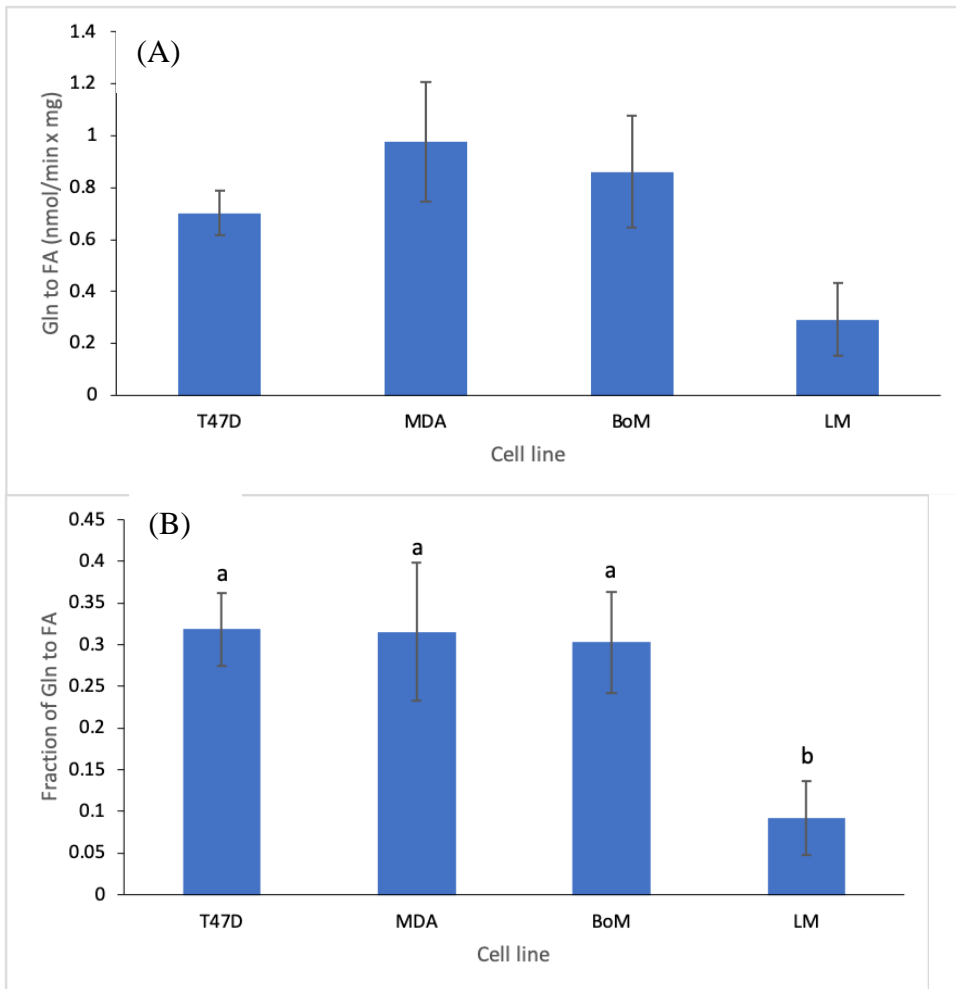
Figure 7 Absolute and fractional rates of C75-sensitive glutamine diverted to fatty acids: (A) The absolute rates of C75-senstive glutamine to fatty acid were calculated as the difference in control and C75 rates. One-way ANOVA indicated no significant cell line effect (p=0.12). (B) The absolute rates in (A) were normalized to the rates of glutamine uptake for the controls. One-way ANOVA indicated a significant cell line effect (p=0.01). Means sharing the same letter are not significantly different.

C. ^{13}C lactate enrichment

Cells were pre-equilibrated for 20-22 h in cell culture media with 1.5 mM 5-^{13}C glutamine and then another 5 h in experimental buffer with 5mM glucose and 1.5 mM 5-^{13}C glutamine to allow isotopic steady-state labeling of intracellular metabolites; control cells run in parallel were incubated with 5 mM glucose and no glutamine to assess background ^{13}C labeling. Compared to controls, all cell lines given ^{13}C-glutamine had significantly less unlabeled (M) lactate and significantly more ^{13}C lactate (Fig. 8A, 8B).

Importantly, virtually all ^{13}C enrichment occurred as the M1 isotopologue (i.e., lactate with a single ^{13}C atom) with virtually none detected as M2 or M3 (Table 2). These results are consistent with the predicted M1-only isotopologue labeling (Fig. 2) that is the basis for the computational model to infer many of the fluxes within our metabolic map (Fig. 1). Furthermore, ^{13}C enrichment in lactate in all four cell lines is consistent with use of glutamine as an anaplerotic substrate to replace TCA cycle malate oxidized by malic enzyme to produce NADPH (Fig. 1). It should also be noted that the fraction of M1 lactate did not increase for any cell line from the first to the second incubation period, suggesting that isotopic steady-state labeling was reached.

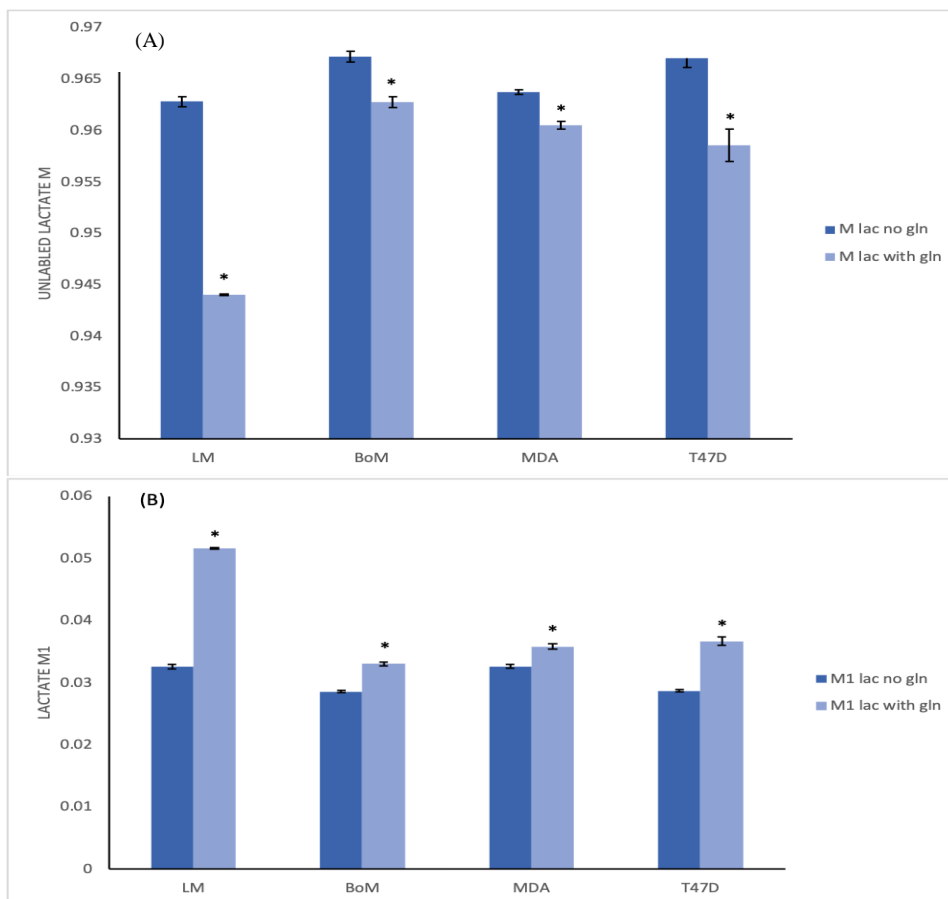*Figure 8 M and M1 lactate content. Cell lines were equilibrated 26-27 h without or with 5-^{13}C glutamine. Fractional ^{13}C lactate content was determined by mass spectrometry. (A) Unlabeled (M) lactate content. (B) Single ^{13}C labeled (M1) lactate content. Data are mean ± standard error of 4 experiments. Asterisks * denote p< 0.05 compared to corresponding control cells this analysis was done by t-test.*

The specific ^{13}C labeling enrichment was determined by subtracting background enrichment (Table 2). LM cells M1 lactate content was 2 to 5-fold greater than the other three lines; T47D cells exhibited intermediate M1 enrichment approximately 2 to 3-fold higher than BoM and MDA cells. A computational model was used to optimize Ratios 1, 2, and 3 to reproduce as closely as possible the measured labeling. For this, the rates of glucose consumption (J_0), lactate production (J_4), mitochondrial respiration (J_{RR}), and glutamine consumption (J_{10}) (see A. Skubiz Honor's thesis for details), together with fractional glucose and glutamine used for fatty acid synthesis, were model inputs that set the constraints for optimizing Ratios 1-3. The model closely reproduced lactate labeling seen for T47D, BoM and MDA cells, but was less effective for the LM line (Table 2). The limitation for the LM line was based on the low measured mitochondrial respiration rate coupled with the high measured M1 lactate enrichment. The respiration rate set a low limit for Ratio 2, and correspondingly this also limited Ratio 3. Nevertheless, the model is a reasonably good fit to these cell lines for estimating glucose and glutamine metabolism.

The model-optimized Ratios are shown in Table 3. The contribution of malic enzyme to pyruvate production differed significantly between cell lines ($p<0.0001$) and was highest for T47D and LM lines; this was expected given that these lines had the highest enrichment of M1 lactate. The contribution of glutamate oxidation (J_{11}) to αKG production differed significantly ($p<0.0001$); both MDA-derived metastatic variants generated the majority of αKG from glutamate (98% for LM and 65% for BoM), suggesting low isocitrate dehydrogenase activity in these cells. The fraction of glutamine

converted to αKG also differed significantly between the lines (p=0.001); the less

aggressive T47D line shunted the highest fraction to αKG (65%), suggesting the more

aggressive LM, MDA, and BoM lines (which shunted 35, 43, and 54%, respectively of

glutamine to the TCA cycle) used a higher proportion of glutamine for protein or small

peptide (e.g., glutathione) synthesis.

Table 2. Measured and Modeled ^{13}Carbon Lactate Enrichment

	Measured ^{13}C Labeling				Predicted ^{13}C Labeling				
	M	M1	M2	M3	M	M1	M2	M3	Model error
LM	0.9819±0.0006[c]	0.0178±0.0006[c]	0.0003±0	<0.0001±0	0.9864±0.0018	0.0136±0.0018	0	0	0.0092±0.0031
BoM	0.9954±0.0002[b]	0.0046±0.0002[b]	<0.0001±0	<0.0001±0	0.9954±0.0002	0.0046±0.0002	0	0	0.0002±0.0001
MDA	0.0066±0.0006[b]	0.0033±0.0006[b]	<0.0001±0.0001	<0.0001±0	0.9966±0.0006	0.0034±0.0006	0	0	0.0006±0.0001
T47D	0.9913±0.0009[a]	0.0083±0.0006[a]	0.0003±0.0001	0.0002±0.0002	0.9916±0.0007	0.0084±0.0007	0	0	0.0011±0.0004

Unlabeled (M), single- (M1), double- (M2), and triple- (M3) ^{13}C labeled lactate produced by cell lines metabolizing 5-^{13}C glutamine was measured by mass spectrometry. Computational modeling was used to reproduce the labeling pattern within the constraints of the measured fluxes J_0, J_4, J_{11}, and J_{RR} (see Fig. 1). Data are the mean ± the standard error of four experiments per cell line. This table compares the measured enrichment with the predicted enrichment from the computational model for ^{13}C labeling. The model error is the sum of the absolute value of the difference between M-M3 predicted and measured. Means that share common letters within a column are not significantly different (significance level p<0.05).

Table 3. Model-optimized flux ratios

	LM	BoM	MDA	T47D
$J_7/(J_{2b}+J_7)$	0.0278±0.0040[a]	0.0132±0.0008[b]	0.0127±0.0021[b]	0.0370±0.0028[a]
$J_{11}/(J_{11}+J_{12f})$	0.9821±0.0131[d]	0.6496±0.0302[c]	0.4988±0.0044[b]	0.4337±0.0092[a]
J_{11}/J_{10}	0.3559±0.0504[c]	0.5381±0.0093[a,b]	0.4350±0.0158[b,c]	0.6518±0.0387[a]

Table 3 Optimized flux ratios from the computational model. Data are means ± the standard error of four experiments. The means that share common letters within a row are not significantly different (significance level p<0.05).

D. Pathway Fluxes

From the model-optimized flux ratios and the measured fluxes (highlighted in red, Table 4), the remaining fluxes for each cell line were determined as detailed in Section F of the methods. Inferred fluxes will be highlighted here, as differences in the measured fluxes have previously been detailed (see A. Skubiz thesis).

Measurement of lactate production alone does not necessarily report aerobic glycolysis if there are glycolysis-independent sources of pyruvate (e.g., malic enzyme). Since malic enzyme's contribution to pyruvate (and by extension, lactate) differed significantly between the cell lines (Table 3), removal of this contribution could impact potential differences in aerobic glycolysis. However, in this case aerobic glycolysis remained not significantly different between the three metastatic lines (MDA, LM, and BoM rates: 31.3 ± 2.1, 30.9 ± 1.0, and 28.2 ± 0.5 nmol lactate/min x mg) but significantly higher than T47D cells (9.47 ± 0.43 nmol lactate/min x mg). Lactate production alone does not assess total glycolysis (glucose to pyruvate) since some glycolytic-derived pyruvate is used for other purposes (e.g., mitochondria oxidation; fatty acid synthesis). Total glycolysis (J_{2c} and J_{2b}) was determined from measurements of mitochondrial respiration rate, lactate production rate, C75-sensitive glucose and glutamine consumption, and glutamine used to support malic enzyme flux. While aerobic glycolysis did not differ between MDA, BoM, and LM cells, total glycolytic flux of MDA cells was significantly greater than BoM cells ($p=0.02$), while LM flux did not differ from either of these lines. The MDA-BoM difference was a consequence of a significantly higher rate of mitochondrial pyruvate uptake (J_5) by MDA cells. Notably, mitochondrial pyruvate uptake for LM and BoM cells was not different, but substantially diverged from their

parent MDA231 cells (Table 4). This trend was also apparent with mitochondrial uptake and oxidation of glycolytic-derived NADH (J_6), and with TCA cycle reaction fluxes (J_{12f}, J_{14}, J_{15}, J_{16}, and J_{17}). These results further suggest significant changes in mitochondrial function between the MDA231 lines and the BoM and LM lines. It is also worth mentioning that the LM TCA cycle did not operate as a continuous cycle as with the other cell lines in that virtually all pyruvate entering was shunted to fatty acid synthesis, so the forward cycle was interrupted from citrate to αKG. However, from αKG to malate the forward cycle was supported by glutamine influx but was again interrupted with virtually no malate being oxidized to oxaloacetate (Table 4); oxaloacetate for citrate synthesis was effectively 'recycled' from that released from citrate used during fatty acid synthesis.

Glucose uptake that was not used for aerobic glycolysis, mitochondrial oxidation, or fatty acid synthesis was assumed to be shunted into the oxidative and non-oxidative pentose phosphate pathways. These experiments did not allow differentiation between these two pathways and so were grouped together as a single pentose phosphate pathway (PPP) flux (Table 4). The MDA and LM PPP fluxes were not different, but both exhibited significantly, or borderline significantly (for LM vs. T47D, p=0.0502) greater fluxes compared to T47D cells. Glucose used by the PPP in the BoM line was no different from the T47D cells, which was unexpected given that demand for de novo nucleotide synthesis is predicted to be higher in the more rapidly proliferating BoM line. When normalized to total glucose uptake rate, BoM glucose shunted to the PPP remained significantly lower than the other three cell lines, which were not different from one another (percent glucose used by PPP for T47D, MDA, LM, and BoM lines was

31.2±3.7%, 23.5±3.0%, 22.5±2.3%, and 12.5±3.1%, respectively); it was surprising that the least metastatic, slow growing T47D line tended toward using the highest proportion of glucose for the PPP.

Finally, malic enzyme activity was approximately two-fold higher in LM cells compared to the other three lines (Table 4). Malic enzyme account for approximately 98% of malate consumption in these cells; by comparison, malic enzyme consumed approximately 21%, 45%, 28% of malate in MDA, BoM, and T47D cells, respectively.

Table 4. Measured and Modeled Fluxes

	T47D	MDA231	BoM	LM
J0 (nmol glc/min x mg)	7.79±0.26[a]	23.1±1.0[b]	16.6±0.53[c]	20.5±0.1[d]
J1+J3 (nmol HxP/min x mg)	2.43±0.33[a,b]	5.44±0.63[c]	2.07±0.59[a]	4.59±0.46[b,c]
J2a	nd	nd	nd	nd
J2b (nmol TrP/min x mg)	10.7±0.5[a]	35.4±2.2[b]	29.1±0.4[c]	31.7±1.1 [b,c]
J2c (nmol 3PG/min x mg)	10.7±0.5[a]	35.4±2.2[b]	29.1±0.4[c]	31.7±1.0[b,c]
J4 (nmol lac/min x mg)	9.83±0.43[a]	31.7±2.0[b]	28.6±0.5[b]	31.8±1.1[b]
J5 (nmol pyr/min x mg)	1.28±0.03[a]	4.15±0.13[b]	0.83±0.07[c]	0.80±0.02[c]
J6 (nmol NADH/min x mg)	0.87±0.03[a]	3.69±0.16[b]	0.44±0.05[c]	0.05±0.05[d]
J7 (nmol mal/min x mg)	0.41±0.03[a]	0.46±0.04[a]	0.39±0.02[a]	0.91±0.15[b]
J8	nd	nd	nd	nd
J9	nd	nd	nd	nd
J10 (nmol gln/min x mg)	1.24±0.12[a]	3.82±0.18[b]	1.66±0.06[a]	3.44±0.27[b]
J11 (nmol glu/min x mg)	0.81±0.05[a]	1.66±0.04[b]	0.89±0.03[a,c]	1.22±0.14[c]
J12f (nmol cit/min x mg)	1.05±0.03[a]	1.67±0.04[b]	0.48±0.07[c]	0.02±0.02[d]
J12r (nmol aKG/min x mg)	0.39±0.04[a,c]	1.21±0.06[b]	0.50±0.02[a]	0.32±0.03[c]
J13 (nmol cit/min x mg)	0.62±0.04[a]	3.68±0.15[b]	0.85±0.03[a,c]	1.09±0.02[c]
J14 (nmol aKG/min x mg)	1.46±0.05[a]	2.13±0.05[b]	0.87±0.09[c]	0.93±0.17[c]
J15 (nmol suc/min x mg)	1.46±0.05[a]	2.13±0.05[b]	0.87±0.09[c]	0.93±0.17[c]
J16 (nmol mal/min x mg)	1.05±0.03[a]	1.67±0.04[b]	0.48±0.07[c]	0.02±0.02[d]
J17 (nmol oaa/min x mg)	1.28±0.03[a]	4.15±0.13[b]	0.83±0.07[c]	0.80±0.02[c]

All fluxes are expressed as nmol of substrate consumed per minute per mg cell protein. Data are mean ± standard error of 4) experiments for each cell line. The red boxes are the measured fluxes. The remaining fluxes were inferred from the computational model optimizing three flux ratios to reproduce the measured

^{13}C enrichment in lactate. Glucose used for the oxidative and non-oxidative pentose phosphate pathways (J_1 and J_3, respectively could not be resolved and so were combined to report overall pentose phosphate flux. Means sharing common superscripts do not significantly differ the significance level $P<0.05$. nd: not determined. Abbreviations: glc: glucose; HxP: hexose phosphates, including glucose-6-phosphate and fructose-6-phosphate; TrP: triose phosphates, including glyceraldehyde-3-phosphate and dihydroxyacetone phosphate; 3PG: 3-phosphoglycerate; lac: lactate; pyr: pyruvate; mal: malate; gln: glutamine; glu: glutamate; cit: citrate; aKG: α-ketoglutarate; suc: succinyl-CoA; oaa: oxaloacetate.

DISCUSSION

The overall goal of this study was to determine if metastatic sub-clones that preferentially invade and grow in lung or bone tissue exhibit metabolic differences from the parent MDA231 breast cancer line. Such metabolic plasticity may be important for tumor growth in different tissue microenvironments, and may guide development of tumor-specific, metabolic-targeted therapies. The major glucose-consuming pathways were quantified with a moderate degree of resolution using the principles of ^{13}C metabolic flux analysis with 5-^{13}C glutamine and unlabeled glucose as substrates. The major finding from this study is that LM and BoM cells exhibit significant metabolic differences from each other and from the MDA231 parent line. Specifically, mitochondrial oxidation of both pyruvate and glutamine is lower in both the LM and BoM lines; consistent with this, less glycolytic NADH is shuttled into mitochondria for oxidation and a greater fraction of glucose is converted to lactate in the BoM and LM lines. Other notable differences include lower PPP flux in BoM cells, lower de novo fatty acid synthesis flux in both BoM and LM cells, and higher malic enzyme flux in LM cells.

Glucose and glutamine are critical nutrients for cancer cell growth. Both of these nutrients can be metabolized to substrates that are oxidized in the TCA cycle to produce ATP. Glucose is transformed to pyruvate through glycolysis which then enters the TCA cycle or is reduced to lactate (4). Pyruvate entering the TCA may be incompletely oxidized and instead used for fatty acid synthesis as acetylCoA derived from the TCA cycle metabolite citrate. In addition to pyruvate, glycolysis generates other metabolites that are substrates for anabolic pathways. Glucose-6-phosphate is oxidized through the oxidative pentose phosphate pathway to produce ribose phosphates for synthesis of

nucleic acids (2) and NADPH for a number of biosynthetic pathways and for protection against reactive oxygen species (ROS). Fructose-6-phosphate and glyceraldehyde-3-phosphate are substrates for the non-oxidative pentose phosphate pathway (running in reverse) that also produces ribose phosphates. Serine and glycine are synthesized from 3-phosphoglycerate; serine can be further metabolized in the folate cycle to support nucleotide synthesis. The majority of glutamine not used for protein synthesis is deaminated within mitochondria to glutamate by glutaminase (GLS). Glutamate is oxidized by glutamate dehydrogenase to the TCA cycle metabolite αKG. The deamination of glutamine to glutamate generates nitrogen (as ammonia) which is used for nucleotide biosynthesis and nonessential amino acids (1). Production of αKG from glutamine is important to replace TCA cycle metabolites removed from the cycle by other reactions. For example, malic enzyme oxidizes malate to pyruvate which can either re-enter the TCA cycle or be reduced to lactate. When malate is oxidized in this way, NADPH is produced which contributes to maintaining the cellular redox state for biosynthetic reactions and protection against ROS. (1). Glutamate is also a substrate for glutathione synthesis; this tripeptide is important for protection against ROS as well as for biosynthetic reactions. Cancer cells have a higher flux of substrates through many anabolic pathways to produce nucleotides, fatty acids and non-essential amino acids necessary for their rapid proliferation. In this way, glucose and glutamine consumption rates are higher in cancer cells. However, different types of cancer cells may exhibit differences in fluxes through specific pathways as a result of differences in either their capacity to transport exogenous nutrients from the extracellular fluid (ECF), their expression of genes coding for different pathways, or the composition of the

ECF/availability of nutrients given the tissue in which the cells proliferate. From this perspective, metastatic cancers that preferentially grow in different organs may do so partly because of metabolic differences.

As expected, the aggressive metastatic MDA231 cell line exhibited significantly greater total glycolytic (glucose to pyruvate) and aerobic glycolytic (glucose to lactate) flux compared to the less metastatic T47D cell line (Fig 9). The importance of increased aerobic glycolysis is likely for generating glycolytic intermediates at a rate sufficient to support anabolic processes (5), but may also be important for adequate supply of ATP. These results are similar to another study showing 2-3 fold higher glucose consumption and lactate production for MDA-MBA-231 cells (6). The high aerobic glycolysis of more metastatic cells is often associated with lower mitochondrial activity; this has often been interpreted that metastatic cells have dysfunctional mitochondria deficient in pyruvate oxidation and ATP synthesis. Surprisingly, we found that MDA231 cells had significantly higher respiration rate and TCA cycle fluxes compared to T47D cells. Pyruvate flux to citrate to meet greater demand for fatty acid synthesis was a notable contributor to the cycle. While the proportion of oxygen used to synthesize ATP was not assessed, greater TCA cycle activity implies that MDA mitochondria are functional and important contributors to cellular ATP synthesis. The higher rates of aerobic glycolysis and mitochondrial respiration and TCA cycle activity imply that MDA cells have a significantly greater ATP demand. While some of this may be due to greater activity of ATP-dependent anabolic pathways, the differences in cell morphology may also contribute. MDA231 cells are more elongated, with many having neurite-like extensions; they also do not adhere together, while T47D cells are more rounded and form tight

clusters. These observations suggest MDA231 cells have a greater plasma membrane surface area:cell volume ratio that would promote greater plasma membrane ion cycling and correspondingly a greater demand for ATP to maintain appropriate ion gradients. Further experiments are required to assess how differences in cell morphology might contribute to ATP demand and whether the efficiency of mitochondrial ATP synthesis differs.

Oxidative/non-oxidative PPP flux was 2.2-fold greater in MDA cells; these cells thus have higher NADPH and pentose phosphate demand for redox homeostasis and nucleotide synthesis than T47D cells (2). Experiments are in progress to resolve the proportion of glucose through the oxidative and non-oxidative pathways It was somewhat surprising that the proportion of total glucose used by the PPP tended to be higher for T47D than MDA cells, (31.2±3.7% vs. 23.5±3.0% of total glucose, respectively; p=0.36) given the more malignant nature of the latter cell line. Some of this difference could be attributed to MDA cells tending to use a greater proportion of glucose for fatty acid synthesis (5.1±1.5% vs. 1.4±1.1%, respectively; p=0.32). Since oxidative PPP flux is subject to strong feedback inhibition by NADPH, MDA231 cells may have less demand for this cofactor. This would most likely derive from less consumption for antioxidant defenses given the greater demand for fatty acid synthesis and potentially other biosynthetic reactions. Glutathione and thioredoxin reductases are major NADPH consumers to protect against ROS; MDA cells could either produce less ROS and so require less NADPH, or have deficits in reductase activities.

Glutamine consumption was 3-fold higher in the MDA cells. One reason for this was to support the significantly higher rate of fatty acid synthesis by reductive

carboxylation of αKG. The flux of both glucose and glutamine to fatty acid is sufficiently

high to indicate MDA cells could be vulnerable by therapeutically targeting this pathway.

However, a significantly greater proportion of glutamine used by T47D cells entered the

TCA cycle (Table 3). This suggests MDA cells preferentially use glutamine for processes

other than resupplying TCA cycle metabolites removed by anabolic reactions; such

processes would include glutamine/glutamate use for protein and glutathione synthesis.

Higher MDA demand for protein synthesis is expected based on the greater proliferation

rate of this cell line. Interestingly, de novo glutathione synthesis is predicted to be

relatively high if MDA cells are deficient in glutathione reductase. Experiments are

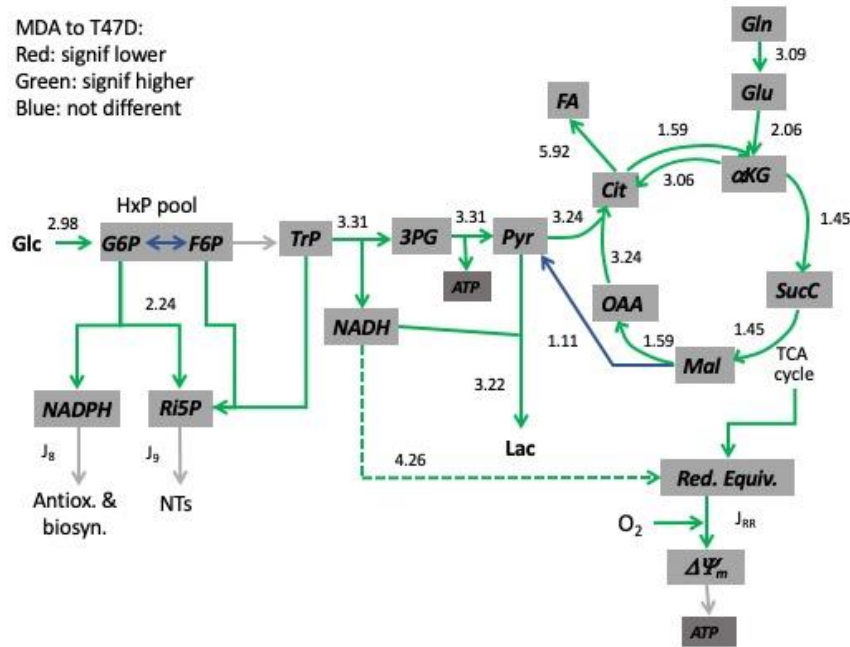ongoing to assess the proportion of glutamine used for glutathione synthesis.

Figure 9: Comparison of MDA231 to T47D fluxes. Numbers are the ratios of MDA to T47D fluxes (Table 3) for each group of reactions. Green and red arrows denote MDA fluxes significantly greater than or less than, respectively, the corresponding T47D fluxes. Blue arrows denote fluxes that were not significantly different.

The malignant LM and BoM subclones exhibit significant metabolic differences

from their parent MDA231 line, which supports our hypothesis and is consistent with

such changes contributing to organ-specific growth of these lines. The most notable

difference is that both lines have significantly lower mitochondrial TCA cycle and

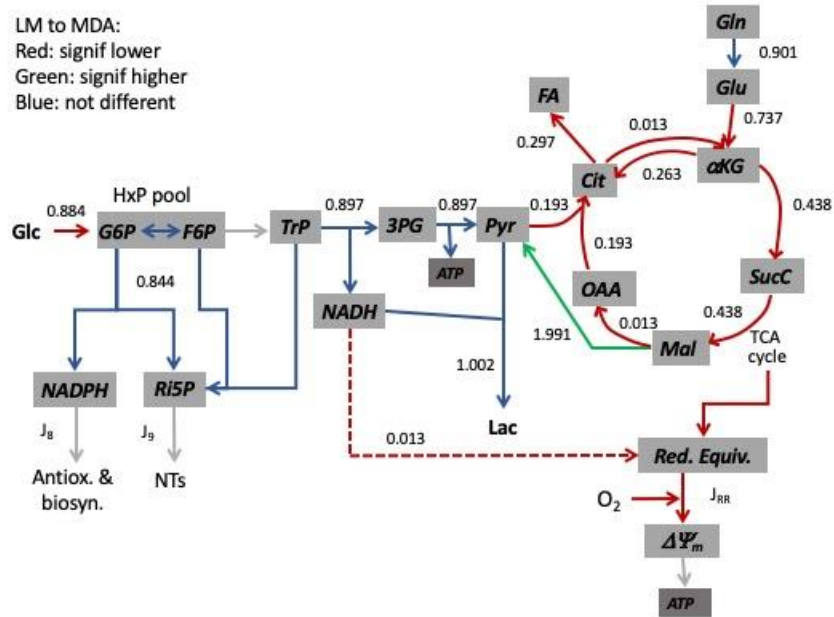respiratory chain activities (Figs 10 and 11).

Figure 10: Comparison of LM to MDA231 fluxes. Numbers are the ratios of LM to MDA231 fluxes (Table 3) for each group of reactions. Green and red arrows denote MDA fluxes significantly greater than or less than, respectively, the corresponding T47D fluxes. Blue arrows denote fluxes that were not significantly different.

Such changes may be particularly important for LM cells that preferentially metastasize

to the lungs, which is a unique organ in two ways- they receive 100% of cardiac output

and thus have the highest blood flow per mass tissue of any organ (Table 5) and have the

highest dissolved oxygen content (P_{O2} approximately 100 mmHg vs. systemic organs

where P_{O2} is approximately 20 mmHg) due to their close proximity to atmospheric air.

Mitochondria are primary producers of ROS through electron leak to oxygen from the

respiratory chain to produce superoxide. The rate of superoxide production partly

depends on the concentration of dissolved oxygen; cells in the lungs are thus more

susceptible to ROS production, and hence to oxidative stress. However, ROS production

also depends on the redox state of the respiratory chain carriers and the TCA cycle

dehydrogenase prosthetic groups (e.g., flavin, thiamine pyrophosphate, and iron-sulfur

groups); the greater proportion of reduced prosthetic groups, the more likely electron leak

to oxygen would occur. These groups can be maintained in a more oxidized state if

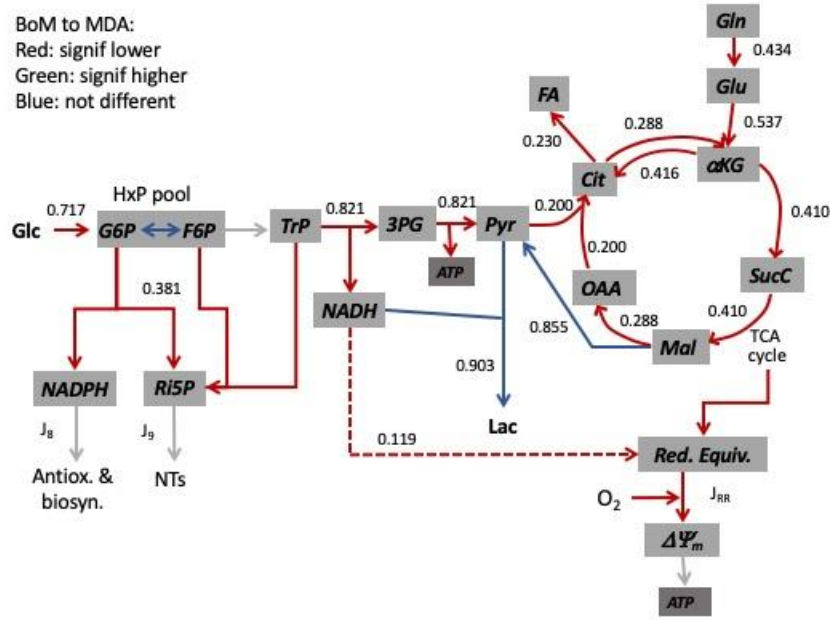substrate supply to mitochondria is restricted.

Figure 11: Comparison of BoM to MDA231 fluxes. Numbers are the ratios of BoM to MDA231 fluxes (Table 3) for each group of reactions. Green and red arrows denote MDA fluxes significantly greater than or less than, respectively, the corresponding T47D fluxes. Blue arrows denote fluxes that were not significantly different.

Consistent with this possibility, LM cells oxidize pyruvate at only 20% the rate of MDA

cells; further, isocitrate dehydrogenase activity is virtually absent, which would not only

eliminate ROS production by this enzyme, but also by αKG dehydrogenase due to further

limiting supply of this substrate. In another experiment, proteomic comparison of MDA-

MB-438 cells and a sub-clone that metastasizes to lung, it was found that peroxiredoxin

overexpression was important for lung metastasis (13). Peroxiredoxin (PRDX2) protects

against oxidative stress by reducing hydrogen peroxide to water (13). By comparison, PRDX2 expression in bone tissue was decreased (13); this is consistent with growth in the lungs requiring adjustments that limit ROS levels. LM cells also shunt the lowest proportion of glutamine to αKG (Table 3); this may also contribute to restricting TCA cycle substrate availability in addition to making more glutamate available for glutathione synthesis. The blunted fatty acid synthesis is likely a secondary consequence of limiting TCA cycle substrate availability; presumably LM cells would have to compensate for this by enhanced reliance on exogenous fatty acids. Increased availability of NADPH by significantly enhanced malic enzyme flux would also reduce oxidative stress. Taken together, these findings are consistent with metabolic adjustments in LM cells to minimize ROS production and oxidative stress in the high oxygen environment of the lungs.

In contrast to the lungs, bone tissue has the lowest blood flow (Table 5). Since blood flow determines the rate at which oxygen, glucose, and glutamine are delivered, BoM metabolism may reflect adaptation to this nutrient-limited environment. These cells use a significantly smaller proportion of glucose for the PPP ($12.2\pm3.1\%$) than the other three lines and have the lowest PPP flux; this is consistent with lower demand for NADPH, possibly due to limited oxygen availability and hence less ROS production. However, these cells proliferate at a rate greater than MDA cells and close to that of LM cells in vitro so it is difficult to understand how the low PPP flux could provide pentose phosphates at a rate adequate to meet the demand for nucleotide synthesis. Low mitochondrial respiratory chain and TCA cycle activities could reflect the limited oxygen supply to bone. They also consume significantly less glutamine than the MDA and LM

lines, which could be a consequence of limited mitochondrial substrate oxidation

capacity. The finding that BoM cells have the highest lactate:glucose ratio further

suggests they rely more heavily on glycolytic ATP production for their energy. In this

respect, BoM cells may be particularly susceptible to therapies that interfere with

glycolysis.

Table 5. Mass adjusted comparison of tissue blood flow rates.

Tissue	Blood flow (ml/min x 100 g tissue)	Reference
Bone	1.5-2.0	Heinonen et al 2013
Dermis (skin)	4-10	Textbook Physiol.
Skeletal muscle	5-10	Textbook Physiol.
Intestine	30	Textbook Physiol.
Brain	57	Textbook Physiol.
Heart	70	Textbook Physiol.
Kidney	350	Textbook Physiol.
Lung	300-500	calculated

CONCLUSIONS

In conclusion, LM and BoM cells exhibit significant metabolic differences from each other and from the MDA231 parent line. This supports our hypothesis of metabolic reprogramming for organ specific growth. TCA cycle and mitochondrial respiratory chain activities are lower for the LM and BoM lines, while both convert a greater fraction of glucose to lactate. Malic enzyme flux was twice as great in LM cells. It appears that LM metabolism has adjusted to minimize ROS levels in the high oxygen content of the lungs by limiting substrate availability to mitochondria while enhancing malic enzyme production of NADPH. These cells may be vulnerable to inhibition of antioxidant defense mechanisms and/or glycolysis. The BoM cells shunted the smallest fraction of glucose through the PPP and the largest fraction to lactate, which could be an adaptation to the low oxygen availability in bone because of the low blood flow to this tissue. These results suggest that LM cells may be vulnerable to inhibition of antioxidant defense enzymes while BoM cells may be more vulnerable to glycolytic inhibition. MDA231 cells were unique in having both high glycolytic and mitochondrial activities, as well as 3-5-fold higher de novo fatty acid synthesis. These cells may be vulnerable to targeted inhibition of fatty acid synthesis. Taken together, these metabolic differences highlight pathways that could help treat tissue-specific metastatic breast cancers.

REFERENCES

1. DeBerardinis RJ, Mancuso A, Daikhin E, Nissim I, Yudkoff M, Wehrli S, et al. Beyond aerobic glycolysis: Transformed cells can engage in glutamine metabolism that exceeds the requirement for protein and nucleotide synthesis. PNAS. 2007;104(49):19345–50. Epub 2007 Nov 21. 10.1073/pnas.0709747104
2. Patra, K. C., & Hay, N. (2014). The pentose phosphate pathway and cancer. *Trends in biochemical sciences*, *39*(8), 347–354. https://doi.org/10.1016/j.tibs.2014.06.005
3. Cluntun, A. A., Lukey, M. J., Cerione, R. A., & Locasale, J. W. (2017). Glutamine Metabolism in Cancer: Understanding the Heterogeneity. *Trends in cancer*, *3*(3), 169–180. https://doi.org/10.1016/j.trecan.2017.01.005
4. Wang, L., Li, J., Guo, L. *et al.* Molecular link between glucose and glutamine consumption in cancer cells mediated by CtBP and SIRT4. *Oncogenesis* **7,** 26 (2018). https://doi.org/10.1038/s41389-018-0036-8
5. Zheng, J. (2012). Energy metabolism of cancer: Glycolysis versus oxidative phosphorylation (Review). Oncology Letters, 4, 1151-1157. https://doi.org/10.3892/ol.2012.928
6. Bartmann, C., Janaki Raman, S.R., Flöter, J. *et al.* Beta-hydroxybutyrate (3-OHB) can influence the energetic phenotype of breast cancer cells, but does not impact their proliferation and the response to chemotherapy or radiation. *Cancer Metab* **6,** 8 (2018). https://doi.org/10.1186/s40170-018-0180-9
7. Minn, A. J., Gupta, G. P., Siegel, P. M., Bos, P. D., Shu, W., Giri, D. D., Viale, A., Olshen, A. B., Gerald, W. L., & Massagué, J. (2005). Genes that mediate breast cancer metastasis to lung. *Nature*, *436*(7050), 518–524. https://doi.org/10.1038/nature03799
8. Minn, A. J., Kang, Y., Serganova, I., Gupta, G. P., Giri, D. D., Doubrovin, M., Ponomarev, V., Gerald, W. L., Blasberg, R., & Massagué, J. (2005). Distinct organ-specific metastatic potential of individual breast cancer cells and primary tumors. *The Journal of clinical investigation*, *115*(1), 44–55. https://doi.org/10.1172/JCI22320
9. Chekhun VF, Todor IN, Lukianova NY, et al. Influence of ferromagnetic nanocomposite (Ferroplat) on human breast cancer cells of different malignancy degrees: pro/antioxidant balance and energy metabolism. Experimental Oncology. 2018 Dec;40(4):268-274.
10. Gupta, G. P., Minn, A. J., Kang, Y., Siegel, P. M., Serganova, I., Cordón-Cardo, C., Olshen, A. B., Gerald, W. L., & Massagué, J. (2005). Identifying site-specific metastasis genes and functions. *Cold Spring Harbor symposia on quantitative biology*, *70*, 149–158. https://doi.org/10.1101/sqb.2005.70.018
11. Hiller K, Metallo CM: Profiling metabolic networks to study cancer metabolism. Curr Opin Biotechnol. 2013, 24: 60-68.

12. Boroughs, L. K., & DeBerardinis, R. J. (2015). Metabolic pathways promoting cancer cell survival and growth. *Nature cell biology*, *17*(4), 351–359. https://doi.org/10.1038/ncb3124

13. Stresing, V., Baltziskueta, E., Rubio, N. *et al.* Peroxiredoxin 2 specifically regulates the oxidative and metabolic stress response of human metastatic breast cancer cells in lungs. *Oncogene* **32,** 724–735 (2013). https://doi.org/10.1038/onc.2012.93

14. Kang Y, Siegel PM, Shu W, Drobnjak M, Kakonen SM, Cordón-Cardo C, Guise TA, Massagué J (2003) A multigenic program mediating breast cancer metastasis to bone. Cancer Cell, 3, 537-549.